2015 International Nuclear Atlantic Conference - INAC 2015
São Paulo, SP, Brazil, October 4-9, 2015
ASSOCIAÇÃO BRASILEIRA DE ENERGIA NUCLEAR - ABEN
ISBN: **978-85-99141-06-9**

FILTER ASSESSMENT APPLIED TO ANALYTICAL RECONSTRUCTION FOR INDUSTRIAL THIRD-GENERATION TOMOGRAPHY

Alexandre F. Velo, João F. T. Martins, Adriano S. Oliveira, Diego V. S. Carvalho, Fernando S. Faria, Margarida M. Hamada and Carlos H. Mesquita.

Instituto de Pesquisas Energéticas e Nucleares (IPEN / CNEN - SP)
Av. Professor Lineu Prestes 2242
05508-000 São Paulo, SP
afvelo@usp.br

ABSTRACT

Multiphase systems are structures that contain a mixture of solids, liquids and gases inside a chemical reactor or pipes in a dynamic process. These systems are found in chemical, food, pharmaceutical and petrochemical industries. The gamma ray computed tomography (CT) system has been applied to visualize the distribution of multiphase systems without interrupting production. CT systems have been used to improve design, operation and troubleshooting of industrial processes. Computer tomography for multiphase processes is being developed at several laboratories. It is well known that scanning systems demand high processing time, limited set of data projections and views to obtain an image. Because of it, the image quality is dependent on the number of projection, number of detectors, acquisition time and reconstruction time. A phantom containing air, iron and aluminum was used on the third generation industrial tomography with 662 keV (^{137}Cs) radioactive source. It was applied the Filtered Back Projection algorithm to reconstruct the images. An efficient tomography is dependent of the image quality, thus the objective of this research was to apply different types of filters on the analytical algorithm and compare each other using the figure of merit denominated root mean squared error (RMSE), the filter that presents lower value of RMSE has better quality. On this research, five types of filters were used: Ram-Lak, Shepp-Logan, Cosine, Hamming and Hann filters. As results, all filters presented lower values of RMSE, that means the filters used have low stand deviation compared to the mass absorption coefficient, however, the Hann filter presented better RMSE and CNR compared to the others. .

1. INTRODUCTION

Unlike the standard aspect of the computed tomography (CT) for medical application, tomography systems for the industrial applications should be adapted to the different size and geometry objects usually placed in an aggressive environment, which contains flammable superheated or corrosive materials, and may be, eventually, subject to high internal pressure: all these factors bring in many difficulties for setting CT devices around the objects (Fig 1) [1,2]. Therefore, the development of special CTs is required, inhibiting its production in large scale. In addition, the industrial systems involve dynamic processes and contain solids, liquids and gases mixtures when CT is an excellent option to see the phases distribution inside the vessels [3,4,5,6,7]. In other words, it is necessary to develop a tomographic system suitable for each purpose in industry [2, 6].

Figure 1: Typical industrial process columns

The CT systems based on transmission use an array of encapsulated radioactive sources and detectors placed in opposite sides of the targeted object. [7,8,9,10]. First generation tomography systems consist of a source emitting a collimated radiation linear beam and a radiation detector (Fig.2a). The source-detector system moves in opposite sides of the object, measuring the attenuation of radiation at each position.

In the second generation CT systems, a set of detectors is placed opposite to a set of radioactive sources, moving (source and detector) around the object under study (Fig.2b).

In the tomography of third generation, the source is collimated so that the path crossed by beams is similar to a fan (Fig.2c). The system moves around the targeted object, obtaining a particular view for an "x" position of the source-detector array. In this type of system, several sources and arrays of multiple detectors may be used.

Finally, the so-called fourth-generation CT systems use a fixed array of detectors (a large number of detectors mounted on a fixed ring) and a radioactive source that moves around the object (Fig.2d). Records of any measure are from the detector, representing a view of the object. However, all CTs are constituted, basically, of same parts: radioactive sources; radiation detectors; a data acquisition system and a suitable computer.

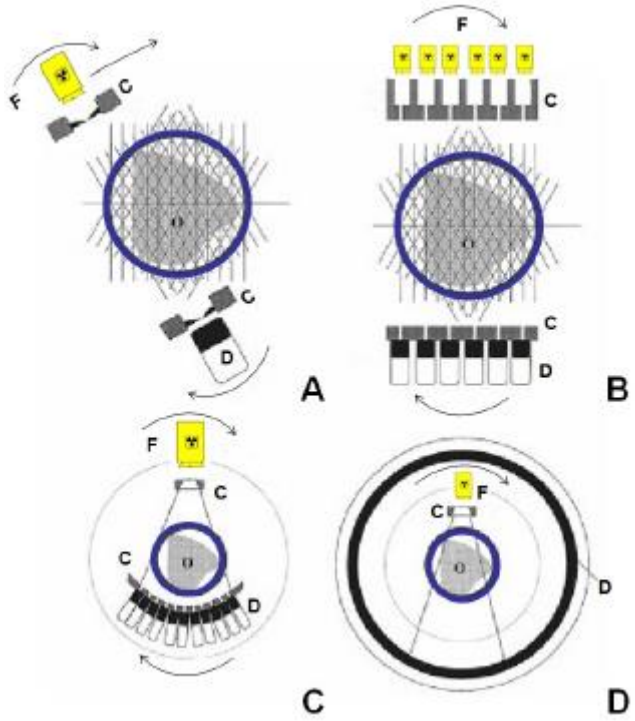

Figure 2: (A) translation - rotation of a beam in parallel (first generation), (B) translation - rotation of multiple sources in parallel (second generation), (C) rotation of a fan-beam (third generation), (D) detector fixed - rotation source (fourth generation). D: detectors; F: source C: collimator, O: object of study.

A third generation computed tomography was developed for analysis of industrial multiphase systems at IPEN [2,11]. In its configuration, an array of three NaI(Tl) detectors is located in an arc concentric to the center of the Cs^{137} gamma source. In order to increase the number of projections measurements in one view of the studied system, the number of detectors in the arc was effectively increased by using a collimator that moves across the detector arc. The whole assembly of the detectors and the radiation source are mounted on a gantry capable of being rotated round the test section axis through a stepper motor interfaced with a host computer. For testing the developed CT, a multiphase phantom was prepared in our laboratory and tomographic experiments were evaluated.

This work consists in reconstruct the images using the back projection reconstruction, applying five types of filters and compare whose filter presented better performance.

2. RECONSTRUCTION PARAMETERS

2.1. Image Reconstruction

The image reconstruction is based on the exponential decay law defined by the equation (1), which is known as Lambert-Beer's law [12]:

$$I=I_0 \cdot e^{\sum_{i=1}^{N} \mu_i \cdot w_{i,\vec{j}}} \qquad (1)$$

where $\boldsymbol{I_0}$ is the initial intensity of the beam radiation that focuses on the object on $\vec{j}$ direction, $\boldsymbol{I}$ is the intensity of the beam radiation through the object, N is the number of pixels on matrix, $\boldsymbol{\mu_I}$ is the mass attenuation coefficient of the matter on pixel $\boldsymbol{I}$ and $w_{i,\vec{j}}$ is the length of the beam radiation through the pixel on pixel $\boldsymbol{I}$ on$\vec{j}$. $w_{i,\vec{j}}$ is defined as weighted matrix element [12].

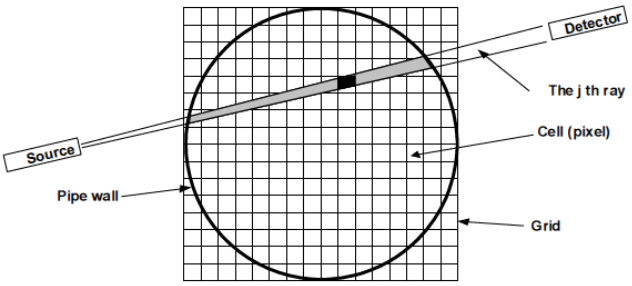

Figure 3: Discretized object [12].

The discretized raysum for each ray j (j = 1, 2, …, J) can be expressed as the equation (2) [12].

$$p_j^{normalized} = \ln\left(\frac{I_{oj}}{I_j}\right) = \sum_{i=1}^{N} w_{ij}\mu_i \qquad (2)$$

where N is the number of pixels. The term w_{ji} represents an element of the weight matrix W, and is defined as the intersectional area between the j^{th} ray and the i^{th} pixel divided by the intersectional area between the j^{th} ray and the sample. The size of W is defined by the number of pixels in the reconstruction grid. Due to Poisson noise corruption of the measured data, a term $\eta_j$describing the noise is added to the equation (3) [12]:

$$p_j^{normalized} = \ln\left(\frac{I_{oj}}{I_j}\right) = \sum_{i=1}^{N} w_{ij}x_i + \eta_j \qquad (3)$$

2.2. Analytical algorithm – Filtered Back-Projection

The Filtered Back Projection (FBP) method is a well-known classical technique [13]. This technique involves the combination of the fast Fourier algorithm with the Radon transformation, though the data is obtained in 2^n parallel rays [13]. The scheme of this algorithm is shown in Fig. 4 [13].

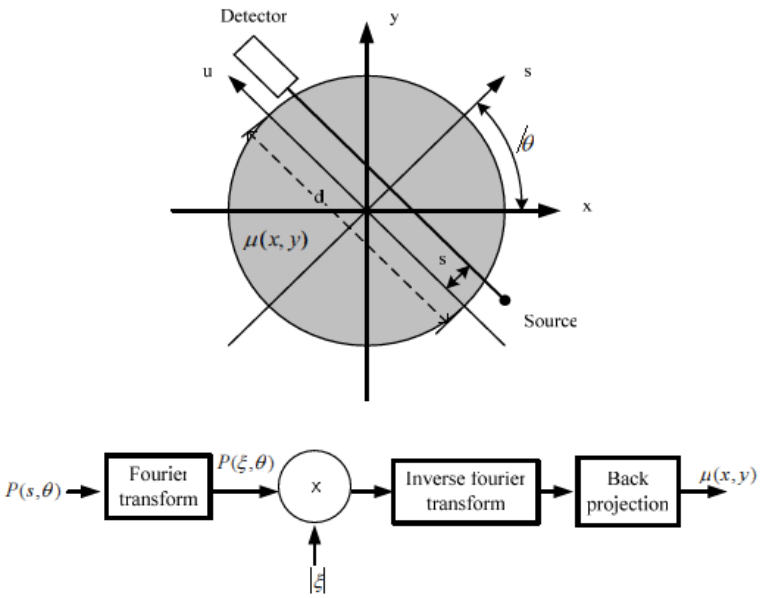

Figure 4: Filtered back projection process [13].

In FBP, the raysum is defined as equation (4).

$$P(s,\Theta)=\frac{1}{d}\ln\left(\frac{p_\theta^0(s)}{p_\theta(s)}\right) \tag{4}$$

where $p_\theta^0(s)$ is measured count with empty object, $p_\theta(s)$ is measured the object, d is diameter of the object [13].

In Fig. 4, $P(\xi,\Theta)$ denotes the Fourier transform of $p(s,\Theta)$. Mathematically, it is expressed as the equation (5) [13]:

$$P(\xi,\Theta)=\int_{-\infty}^{\infty} P(s,\Theta)\exp(-j2\pi\xi s)\,ds \tag{5}$$

where $\hat{p}(s,\Theta)$denotes the inverse Fourier transform of $P(\xi,\Theta)\bullet|\xi|$, and it is represented mathematically as presented on equation (6) [13].

$$\hat{p}(\xi,\Theta)=\int_{-\infty}^{\infty} |\xi|P(\xi,\Theta)\exp(j2\pi\xi s)\,d\xi \tag{6}$$

The reconstructed image can be obtained from a back projection of $\hat{p}(\xi,\Theta)$. The reconstruction is presented by equation (7) [13].

$$\mu(x,y)=\int_0^{\pi} \hat{p}(x\cos\Theta+y\sin\Theta)d\Theta \tag{7}$$

This method is called filtered back projection (FBP). The FBP algorithm is well established process and strictly based on mathematical theory. The advantage of FBP is that it needs less computation demands when compared to the iterative method [13].

The projections data were reconstructed with five different filters: Ram-Lak, Sheep-Logan, Cosine, Hamming and Hann filters. Each filter was defined to modify the ideal Ramp filter in the frequency domain, equation (8) [14].

$$H(\omega) = |\omega| W(\omega) \tag{8}$$

where ω is the spatial frequency and W(ω) is defined according each filter. For Ram – Lak filter, Sheep – Logan, Cosine, Hamming and Hann, W(ω) is defined by the equations (9) – (13) respectively [14].

$$W(\omega) = \text{rect}(\omega/2) \tag{9}$$

$$W(\omega) = \text{rect}(\omega/2)\text{sinc}(\omega/2) \tag{10}$$

$$W(\omega) = \text{rect}(\omega/2)\cos(\omega/2) \tag{11}$$

$$W(\omega) = \text{rect}(\omega/2)(0.54 + 0.46\cos(\omega)) \tag{12}$$

$$W(\omega) = \text{rect}(\omega/2)(0.5 + 0.5\cos(\omega)) \tag{13}$$

For the five filters, the amplitudes as function of frequency are described in Fig. 5.

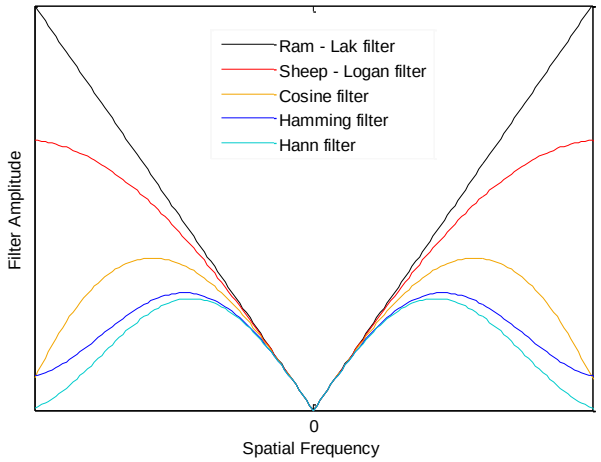

Figure 5: Amplitude as a function of spatial frequency for various reconstruction filters.

2.3. Image Quality Control

Traditionally is used the parameter called Figure of Merit defined as the Root Mean Square Error which represents a value calculated by the equation (14) [15, 16].

$$\mathrm{RMSE(N)} = \sqrt{\frac{\sum_{i=1}^{N}(\mu_i - \hat{\mu}_i)^2}{N}} \tag{14}$$

where μ_i is the observed mass attenuation coefficient value for the i^{th} pixel and $\hat{\mu}_i$ is the respective true value, N is the number of pixels. The RMSE parameter represents the standard deviation between the evaluated pixel to the expected one. The standard deviation is a parameter that expresses the dispersion of the measures of a normal population (Gauss curve), defined by equation (15) [16].

$$f(\mu,\hat{\mu}) = \frac{1}{\sigma\sqrt{2\pi}} \cdot e^{-\frac{(\mu-\hat{\mu})^2}{2\sigma^2}} \tag{15}$$

where $\sigma = \mathrm{RMSE}$ is the standard deviation.

The dispersion of $\mu - \hat{\mu}$ not always obey a normal distribution and therefore the RMSE parameter does not adequately represent the measure of the dispersion function $f(\mu, \hat{\mu})$ [17]. The percentiles of $\tilde{\mu}_{q_{25\%}}$ and $\tilde{\mu}_{q_{75\%}}$ would be more indicated to express the dispersion of this function. As these aspects are not consolidated on literature, the RMSE parameter is still used to compare the quality of the reconstructed images by the algorithm of tomographic reconstructions.

As a proxy for image quality, the contrast-to-noise ratio absorption is performed as the equation (16).

$$\mathrm{CNR} = \frac{|\bar{X}(im) - \bar{X}(BG)|}{\sqrt{\sigma^2(im) + \sigma^2(BG)}} \tag{16}$$

where $\bar{X}(im)$ is the mean of the Region of Interest on the structure and the $\bar{X}(BG)$ is mean of the image background.

3. EXPERIMENTAL PROCEDURE

Tomography measurements were performed using the third generation CT developed at the CTR/IPEN [2,11]. Each of the three 2" NaI(Tl) detectors has an individual collimator made in lead, so that the detectors are completely shielded by the collimator. Each collimator has a hole of 5 mm diameter for sampling beams. These dimensions for the collimator holes were optimized based on considerations of providing adequate area for detecting photons with good statistic into the chosen sampling period. The radioactive sealed Cs^{137} (662 keV) source is 3.7 GBq placed inside a lead collimated shield system providing a 45° fan beam arc Fig. 6.

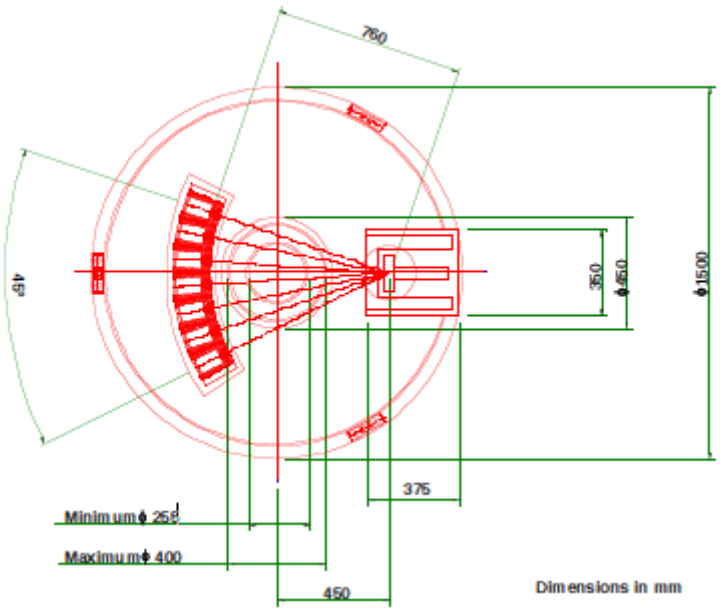

Figure 6: Top view drawing of the iCT used.

A multiphase phantom was designed and prepared in order to be able of varying the proportions of the phases (gas, liquid or solid) to validate the third generation tomography developed at CTR/IPEN. The 15 cm diameter phantom consists of polymethylmethacrylate solid containing three holes one filled with a steel plug another with an aluminum plug and the third one empty, as illustrated in Fig. 7. The idea was to switch the gas and liquid phases, while maintaining the solids fixed.

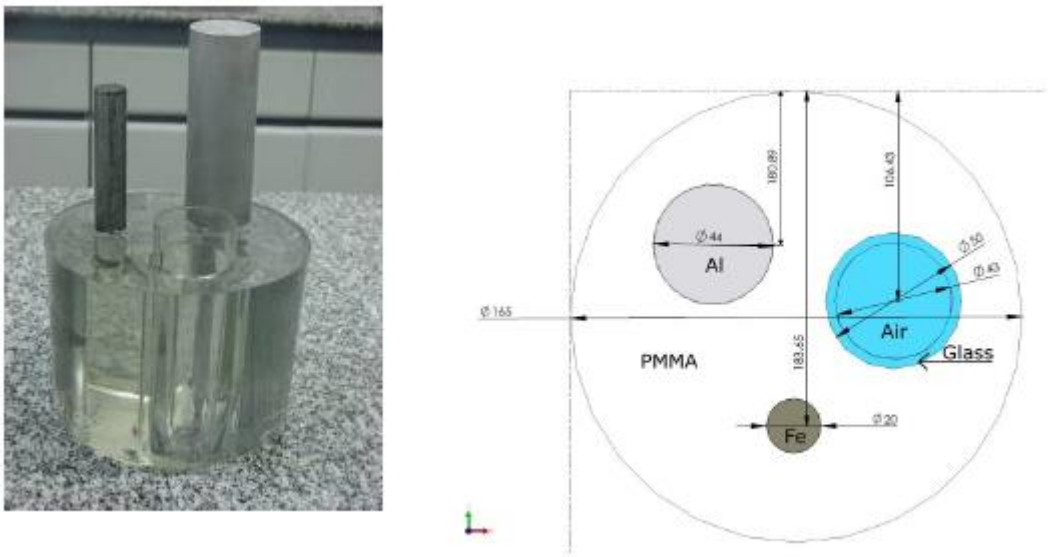

Figure 7: Picture of the multiphase phantom.

The array of seven NaI(Tl) detectors and the Cs^{137} source were placed on the rotatable gantry and the phantom was installed in the center between the array of detectors and the source. The gantry can be rotated around the axis of the phantom by a stepping motor that is

controlled through a microprocessor. The size of the array of detectors is sufficiently large so that the entire phantom was within the field of view of the detectors all the time. Moreover, the whole assembly can be moved in the axial direction along the phantom to perform a scan at different axial levels of the phantom. Fig. 8 shows an illustration of the third generation CT with the phantom in the center of the gantry. The data acquisition board and the mechanical control used were developed at CTR/IPEN also [2,11].

Figure 8: Set-up of the third generation CT.

The tomographic measurements were carried out using the multiphase phantom prepared at IPEN (Fig. 7). To obtain statistically significant results, and to reduce the effect of the position the CT scans were obtained rotating around the phantom the plate with the source and detectors 360° in 60 views, each view provided 6°. The movement of the detector–collimator assembly was controlled by another step motor, in each movement, this assembly rotated by 0.39° generating 53 projection per detector or 159 (53x3) projections per view totalizing 9540 projections per image. Previously, each NaI(Tl) detector was evaluated by gamma spectrometry techniques using an associated multichannel electronics and data acquisition board developed by CTR/IPEN [17].

To compare the results of the linear attenuation coefficients of the phantom components is necessary to know the value these coefficients for pure materials (pure phase). Hubell & Seltzer (1996) created a database called NIST [18], where figures are available for the attenuation coefficients as a function of energy for a specific compound or material. In these experiments, the effective linear attenuation values were determined using densitometry, a procedure consists of the direct application of the Lambert-Beer equation (1) using in only one detector, where the material to be measured is placed in the path of the radiation.

4. RESULTS AND DISCUSSION

The reconstructions images by the filtered back-projections are presented on the Fig. 9. First column represents the sinogram of the images, where the first sinogram no filter was applied, the second is the sinogram with the Ram-Lak filter, the third with Sheep-Logan filter, the fourth whit the Cosine filter, the fifth with the Hamming filter and the last one with the Hann filter. Second column represents the theoretical images used to compare to the reconstructions ones. Third column is the images reconstructed, the fourth is the RMSE values and the last column is the CNR for each image.

Sinogram	Theroretical Image	FBP	RMSE(N)	RMSE(μ)	CNR
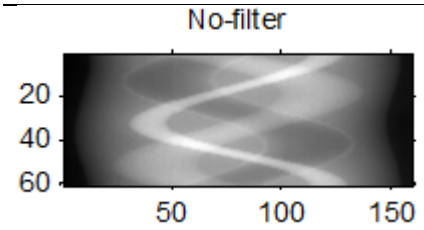	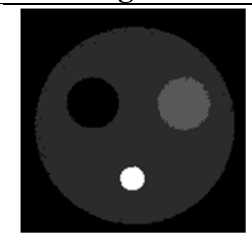	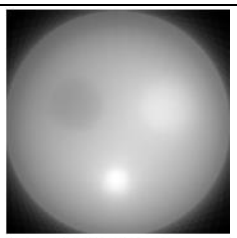	6.0417	30.528	2.8152
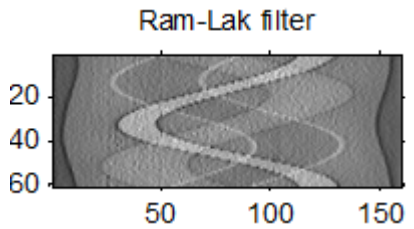		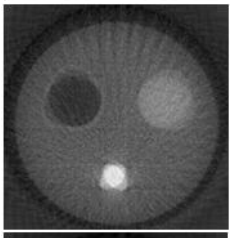	0.0325	0.1643	2.9081
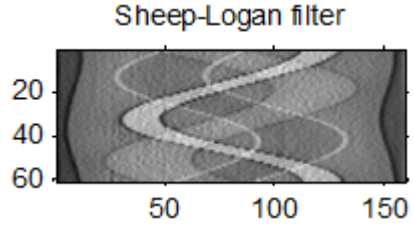		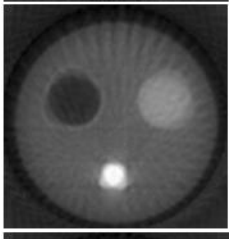	0.0323	0.1632	4.2128
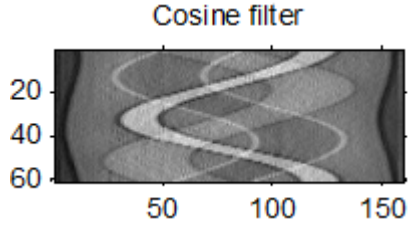		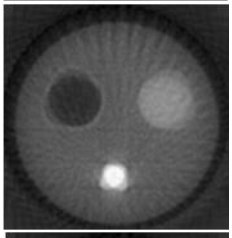	0.0322	0.1626	6.6008
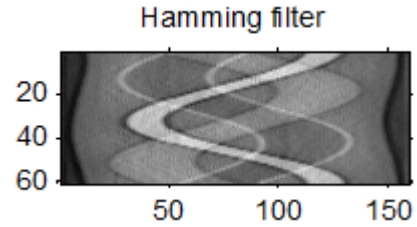		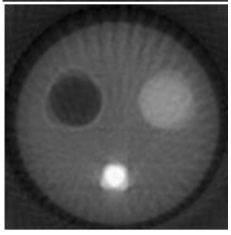	0.0322	0.1626	8.2665
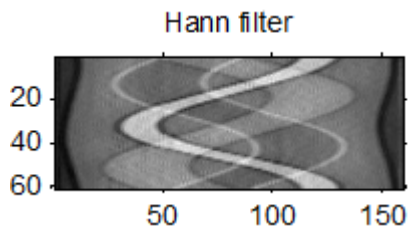		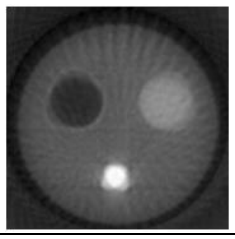	0.0322	0.1626	8.9854

Figure 9: Results of the filter application, FBP, RMSE and CNR

On a subjective analysis, Fig. 9 shows that the reconstruction by back projection gets enhanced when a filter is applied. On an objective analysis, the high results of the RMSE and the low CNR values for the sinogram with no filter emphasize that the image needs an enhancement.

When the filter is applied, the values of the RMSEs decreases compared to the RMSE with no filter. Although the RMSE values of the images with filters is very close to each other, the RMSE value for the last three filters (Cosine filter, Hamming filter and Hann filter) is smaller than the others two (Sheep Logan and Ram-Lak), which suggests that this three images has better coherence compared to the theoretical image, however these three images have the same RMSE value.

Analysing the CNR values, it is possible to observe that the values is different for different filters. Even the Cosine filter, Hamming filter and Hann filter presents the same RMSE value, the Hann filter has better CNR compared to the other filters, this means that the Hann filter had better performance compared to the others filters, since it had the smaller RMSE value and the highest CNR value.

5. CONCLUSIONS

By the Fig. 9, it is possible to observe that the reconstruction by back projection gets enhanced when a filter is applied.

All filters presented coherence with the theoretical image, since the RMSE values of the filtered images is very close to zero. Even the Cosine filter, Hamming filter and Hann filter presents the same RMSE value, the Hann filter has a higher CNR, which means that this filter filters filtered the noise better than the others, enhancing the contrast (Fig.9).

Hence, for this type of reconstruction, using the back projection, the Hann filter is more indicated to use on the sinogram, where this filter makes the reconstructed image approach to the theoretical image, and enhance the contrast decreasing the noise of the image.

ACKNOWLEDGMENTS

The authors express their acknowledgment to CNEN for the financial support. The authors, Carlos Henrique de Mesquita and Margarida Mizue Hamada thank for their fellowship.

REFERENCES

1. KUMAR, S. B.; DUDUKOVIC, M. P., Computer-assisted gamma and X-ray tomography: Application to multiphase flow In Non-Invasive Monitoring of Multiphase Flows; Chaouki, J., Larachi, F., Dudukovic´, M. P., Eds.; Elsevier: Amsterdam, The Netherlands, 1997; Chapter 2, p 48.

2. MESQUITA, C. H.; VASQUEZ, P. A. S.; HAMADA, M. M. Multi-source third generation computed tomography for industrial multiphase flows applications. In:

2011 IEEE Nuclear Science Symposium Conference Record, Oct. 2011 (in press).

3. MESQUITA, C. H.; DANTAS, C.R., COSTA, F.E.; CARVALHO, D.V.S.; MADI, T. F; VASQUEZ, P. A. S.; HAMADA, M. M. Development of a Fourth Generation Industrial Tomography for Multiphase Systems Analysis. In: 2010 IEEE Nuclear Science Symposium Conference Record, pp. 19-23, Oct. 2010.

4. KUMAR, S. B.; DUDUKOVIC, M. P., Gas holdup in bubble columns at elevated pressure via computed tomography. Int. J. Multiphase Flows, vol. 27, pp.929-946, 2001.

5. ISMAILA; GAMIOG, J. C., Tomography for rmulti-phase flow measurement in the oil industry. Flow Measurement and Instrumentation, vol. 16, pp. 145-155, 2005.

6. VASQUEZ, P. A. S. ; MESQUITA, C. H. ; HAMADA, M. M. . Methodological Analysis of Gamma Tomography System for Large Random Packed Columns. Applied Radiation and Isotopes, v. 68, p. 658-661, 2010.

7. IAEA-TECDOC-1589 Industrial Process Gamma Tomography, Viena, Maio 2008.

8. VASQUEZ, P. Análise de sistemas multifásicos utilizando tomografia computadorizada gama monoenergética e polienergética. 2008 Tese (Doutorado) –IPEN-USP, São Paulo.

9. CHAOUKI, J.; LARACHI, F.; DUDUKOVIC, M. Noninvasive Tomographic and Velocimetric Monitoring of Multiphase Flows. Ind. Eng. Chem. Res., v. 36, p. 4476-4503, 1997.

10. JOHANSEN, G. A.; JACKSON, P., Radioisotope Gauges for Industrial Process Measurements. 2004 John Wiley & Sons, Ltd. ISBN 0-471-48999-9.

11. CALVO, W. A. P.; HAMADA, M. M; SPRENGER, F. E.; VASQUEZ, P. A. S.; RELA, P. R.; MARTINS, J. F. T.; PEREIRA, J. C. S. M.; OMI, N. M.; MESQUITA, C. H., Gamma-ray computed tomography Scanners for applications in multiphase system columns. Nukleonika,; v. 54(2), p. 129-133, 2009.

12. MAAD R., Design Optimization of High Speed Gamma-Ray Tomography. A dissertation submitted in partial fulfilment of the requirements for the degree of Doctor of Philosophy in Physics. Department of Physics and Technology University of Bergen Norway., 2009.

13. IAEA – TECDOC 1589, Industrial Process Gamma Tomography, may 2008.

14. LEE S.W., LEE C. L., CHO H. M., PARK H. S., KIM D. H., CHOI Y.N. CHOI AND KIM H. J. Effects of Reconstruction Parameters on Image Noise and Spatial Resolution in Cone-beam Computed Tomography. Journal of the Korean Physics Society, v. 59, n. 4, pp. 2825~2832, 2011.

15. MAAD, R., JOHANSEN G.A., Experimental analysis of high-speed gamma-ray tomography performance. Meas. Sci. Technol. 19, 1-10, 2008.

16. VASQUEZ P. A.S., VARMA R., HAMADA M. M., MESQUITA C.H., AL-DAHHAN M.H., Image Reconstruction Algorithms applied to Polyenergetic Gamma Ray Tomography for Large Systems. 6th International Symposium on Process Tomography., 2012.

17. MESQUITA C.H., VASQUEZ P. S., CALVO W. A.P., MARCATO L. A., CARVALHO D. V. S., MARTINS J. F. T., SANTOS R. A. and Margarida M. HAMADA M. M., Multi-Source Third Generation Computed Tomography for Industrial Multiphase Flows Applications., pp. 1-9, 2010.

18. HUBBELL, J. H.; SELTZER, S. M., Tables of X-Ray Mass Attenuation Coefficients and Mass Energy-Absorption Coefficients. National Institute of Standards and Technology (NIST), 1996 (http://physics.nist.gov/PhysRefData) INAC 2011, Belo Horizonte, MG, Brazil.